



# Investigation of joints from laser powder fusion processed and conventional material grades of 18MAR300 nickel maraging steel

W. Tillmann<sup>1</sup> · L. Wojarski<sup>1</sup> · T. Henning<sup>1</sup>

Received: 17 November 2020 / Accepted: 15 February 2021  
© The Author(s) 2021

## Abstract

Even though the buildup rate of laser powder bed fusion processes (LPBF) has steadily increased in recent years by using more and more powerful laser systems, the production of large-volume parts is still extremely cost-intensive. Joining of an additively manufactured complex part to a high-volume part made of conventional material is a promising technology to enhance economics. Today, constructors have to select the most economical joining process with respect to the individual field of application. The aim of this research was to investigate the hybrid joint properties of LPBF and conventionally casted 18MAR300 nickel maraging steel depending on the manufacturing process and the heat treatment condition. Therefore, the microstructure and the strength of the hybrid joints manufactured by LPBF or vacuum brazing were examined and compared to solid material and joints of similar material. It was found that the vacuum-brazed hybrid joints using a 50.8- $\mu\text{m}$ -thick AuNi18 foil provide a high tensile strength of 904 MPa which is sufficient for a broad field of application. Furthermore, the additively manufactured hybrid samples offered with 1998 MPa a tensile strength more than twice as high but showed a considerable impact of buildup failures to the strength in general.

**Keywords** Economical manufacturing · Joining · Nickel maraging steel · Laser powder bed fusion (LPBF) · Vacuum brazing · Joint strength

## 1 Introduction

Nickel maraging steels are low-carbon tool steels containing 18% of nickel and high amounts of cobalt and molybdenum beside smaller amounts of titanium and aluminum. Common tool steels like AISI H11 are hardened by austenizing and quenching so that there will be a martensitic microstructure due to a limited diffusion ability of carbon. In contrast to that,

the hardening mechanism of nickel maraging steels is based on precipitation hardening by the formation of  $\text{Ni}_3\text{Mo}$  and  $\text{Ni}_3\text{Ti}$  phases during an annealing process which is also called martensitic ageing [1]. The different grades of nickel maraging steels are primarily characterized with regard to the yield strength which is improved by increasing contents of cobalt, molybdenum, and titanium. In detail, cobalt reduces the solubility of molybdenum so that the amount of  $\text{Ni}_3\text{Mo}$  precipitations is increased just as significantly as the hardness and the strength. Nickel maraging steels offer with a tensile strength of up to 2400 MPa as well as a remarkable low temperature toughness uniquely good mechanical properties so that this material is used for example for highly stressed structural components like wind tunnel models, for hydraulic chucks, or for injection and die casting molds [2]. LPBF processes using nickel maraging material are very well researched and established in industry [1, 3–5].

Today, cost efficiency is a main point of a manufacturing process and the costs of a conventionally casted nickel maraging steel can be estimated to be about ten times higher

---

Recommended for publication by Commission XVII - Brazing, Soldering and Diffusion Bonding

---

✉ T. Henning  
Tim.Henning@tu-dortmund.de

W. Tillmann  
Wolfgang.Tillmann@tu-dortmund.de

L. Wojarski  
Lukas.Wojarski@tu-dortmund.de

<sup>1</sup> Institute of Materials Engineering, Faculty of Mechanical Engineering, TU Dortmund University, Dortmund, Germany

than the common tool steel AISI H11. In order to point out the economical factor clearly, the costs of the nickel maraging LPBF powder used in the present research was about twice as the conventionally casted material of the same grade. If one also considers the fact that powder bed fusion is a fairly slow layer by layer process, it becomes evident that the total manufacturing costs are much more dependent of the LPBF process time than of the material costs itself [6–8]. Even the development of more powerful lasers and the advancement to multiple laser systems were still not able to fundamentally change this fact in the last years [8, 9]. Nevertheless, the freedom of design is very high and the production of near-net shaped parts with multidimensional surfaces and the integration of precise and complex cooling channels have changed impressively the market of tooling [10–12]. As a direct consequence of these explanations, even today large-volume parts cannot be produced economically by LPBF [6, 13]. If there is an unavoidable need to do so, there will be extremely high machine hour rates or the hull-and-core strategy is applied as a compromise [14]. In that case, the outline of the part is buildup detailed with a small laser focus and thin layers to achieve a precise dimensional accuracy, whereas a large laser focus as well as thick layers are used for the core with acceptance of a substantially lower quality [15, 16]. Hence, it is obvious to use a conventionally casted part wherever it is possible [17]. If a complex shaped segment of a tool is manufacturable by LPBF more economically compared to classic machining, the volume of this segment should be minimized by the design of hybrid components [18].

There are three main manufacturing methods to realize such highly stress-resistant hybrid components consisting of a complex-shaped functional part and of an easy workable full body part like it is conceivable in example for clamping surfaces [19, 20]. First, laser powder bed fusion can be directly processed on top of the conventional bulk surface leading to an additively manufactured joint [11, 13, 18]. In this context, a post-weld heat treatment is advisable to set the material properties in a defined way, to reduce residual stresses, and to adjust the microstructure and the properties of the two segments as far as possible [21–24]. In contrast to conventionally casted materials, the microstructure of parts produced by LPBF is very fine cellular and non-equiaxial in the as-build condition [1]. Secondly, vacuum brazing of preprocessed LPBF parts is particularly attractive, if there will be more joining surfaces at the same time or the joint geometry is not processable exclusively by additive manufacturing [25]. Furthermore, a sustainable advantage might be achievable with respect to the total manufacturing time if the heat treatment, which consists of solution annealing and precipitation hardening, is combined with the joining by brazing in a single furnace run [2, 26, 27]. A third production method for hybrid parts is characterized by diffusion bonding, but in this case, the usability is highly limited by the challenge of load

application on complex shaped surfaces. In addition to this, there should be a separate precipitation hardening process due to usually high operating costs of the furnace [11]. The objective of this research is to evaluate the attainable strength properties of hybrid joints produced by LPBF or vacuum brazing. This is of high interest for engineers and constructors in order to select a cost-efficient and suitable manufacturing technology for individual tools depending on the geometry, quantity, and load conditions [28].

## 2 Materials

AISI 18MAR300 was used as gas atomized powder with a particle size of +45–15  $\mu\text{m}$  provided by Carpenter Additive for laser powder bed fusion. As shown in Table 1, the LPBF powder contains slightly higher amounts of cobalt, nickel, and molybdenum, as well as more impurities of carbon, oxygen, and aluminum, compared to chemical composition of the conventional casted rod material. For the vacuum brazing, a 50.8- $\mu\text{m}$ -thick AuNi18 foil was utilized which has a eutectic melting temperature of 955  $^{\circ}\text{C}$ .

## 3 Experimental procedures

In the following, the experimental procedure and the analysis methods used are explained in detail.

### 3.1 Experimental design

In this contribution, LPBF was processed on top of conventionally casted as well as on top of prefabricated LPBF parts in the as-build condition. The latter were used to examine the joint area of two-step processed samples which may occur if the process interrupts overnight or one part have to be

**Table 1** Comparison of the chemical composition of the conventionally casted material and the LPBF powder of AISI 18MAR300

[wt.-%]	Conventional casted	LPBF powder
C	0.002	0.030
O	-	0.02
Al	0.04	0.10
Ti	1.02	1.00
Cr	0.06	0.01
Mn	0.02	0.02
Fe	Balance	Balance
Co	8.79	9.80
Ni	17.19	18.90
Mo	4.73	5.20

designed in addition to an already existing component for example to repair locally worn areas of a tool. Furthermore, the effect of a vacuum furnace heat treatment by solution annealing and precipitation hardening was investigated for these samples and compared to single-processed ones as well as to the heat-treated conventional material. In addition, a vacuum-brazing process was designed to produce LPBF/LPBF, LPBF/Conv. and Conv./Conv. joints for which the heat treatment and the brazing were conducted in a single furnace run. As stated in the literature and also proven by proper preliminary investigations, the brazing temperature should not exceed 975 °C; otherwise, a significant growth of the austenitic grains will highly affect the low temperature toughness [29]. In this regard, the eutectic brazing alloy AuNi18 was selected in foresight to obtain higher strength properties of the joints than it is accomplishable with cheaper silver-based brazing alloys like the eutectic AgCu28 or AgCuPd alloys [2, 27, 30]. All the previously explained samples were characterized by means of microstructure analysis and hardness indentation as well as by tensile testing and increasing load fatigue testing.

In Table 2, an overview of the conducted experiments is illustrated for the multifarious of joined components from LPBF and conventional material, which were examined comparatively as well as in dependence on the process of manufacturing and on the state of the heat treatment.

The number of samples was set to one for microstructural analysis, to three for tensile testing, and to five for increasing load fatigue testing. A cylindrical geometry with a diameter of 22 mm and a height of 110 mm was used for the solid samples. In case of the LPBF/LPBF joints, a prefabricated LPBF cylinder of diameter 22 mm and height 55 mm was used in the as-built condition to process the top part with the same geometry. It is vital to know that at least 2 mm of the top of the preprocessed LPBF cylinder was finally removed by grinding to get rid of the outer layer which contains usually high residual stresses and oxidization. In case of the LPBF/Conv. joints, the diameter of the LPBF part was reduced to 20 mm in order

to match the alignment of the machine. In regard to saving material costs, the height of the samples for the microstructural analysis was set to 15 mm for each part. Prior to brazing, the LPBF samples used for this were machined to cylinders of diameter 18 mm and height 50 mm, which was the same geometry for the conventional part. A cylinder of diameter 16 mm and height 15 mm was brazed on top of a cylinder of diameter 18 mm and height 15 mm for metallographic inspection.

### 3.2 Manufacturing of the LPBF samples

Laser powder bed fusion was carried out by the direct manufacturing research center (DMRC) on a DMG Mori LT30 machine with a preheat temperature of 200 °C, a laser power of 275 W, and a spot size of 75 µm. Furthermore, a strip exposure of 6 mm and a hatch distance of 115 µm were used with rotation of 67° for each layer with a thickness of 50 µm. During the process, argon was used as a shielding gas with a residual share of oxygen of around 0.1 vol-%. In case that the process was started on top of an existing part, there was indeed no support structure printed. The heat treatment of solution annealing and precipitation hardening was completely the same for the LPBF samples as described for the brazed samples in the following, except of the additional heating to the brazing temperature after solution annealing.

### 3.3 Manufacturing of the vacuum-brazed samples

Brazing was carried out in a horizontal vacuum furnace type EU 80/1H (Schmetz Inc.). The samples were arranged in a fixture to assure the axial alignment but no additional weight was used. After evacuating the recipient to a vacuum better than  $3.4 \cdot 10^{-6}$  kPa, the samples were heated to 650 °C with 10 °C/min which was set as a standard heating rate in this process. Following a dwell time of 15 min to heat through the batch, the samples were solution annealed for 1 h at 830 °C. After brazing at 975 °C for 15 min, the batch was cooled down

**Table 2** Experimental design of solid material and joined compounds considering the heat treatment condition

Sample type	Heat treatment condition	
Solid material	LPBF	As-built
	LPBF	Solution annealed and precipitation
	Conv.	hardened
Additively manufactured (AM) joints	LPBF/LPBF	As-built
	LPBF/Conv.	Solution annealed and precipitation
	LPBF/Conv.	hardened
Vacuum-brazed joints	LPBF/LPBF	Brazing included in the solution
	LPBF/Conv.	annealing and precipitation
	Conv./Conv.	hardening process

to 75 °C with a convective nitrogen cooling gas flow of 200 kPa in order to save a significant amount of operating time compared to vacuum cooling which is also possible for maraging steels. Then, the samples were instantaneously precipitation-hardened for 3 h at 510 °C, cooled down slowly by just 2 °C/min to 300 °C, and then again fast by a nitrogen overpressure of 200 kPa again. In detail, the process step of slow cooling was conducted to fulfill the recommendations for a post-weld heat treatment of powder bed-fused 18MAR300 parts in regard to limiting the cooling stresses within the hardened microstructure.

### 3.4 Tensile testing and increased load fatigue testing

The samples for strength characterization shown in Fig. 1 were machined according to the specification DIN EN ISO 6892-1:2009-12 to type B10x50 by hard turning with a GS200MSY (Hardinge Inc.). Water cooling was used in order to limit the heat input into the samples. In case of the joined samples, the fusion zone was located in the center.

The strength characterization was carried out with a 250-kN servohydraulic pulse testing machine type 8802MTM1021 (Instron Inc.) with a testing speed of 0.025 mm/s. Three samples were used to determine the average tensile strength where in addition the half of this value was set as initial load for the increasing load fatigue testing on five samples each. In every load increment,  $10^4$  cycles with a frequency of 10 Hz and an amplitude of  $\pm 10$  MPa were applied after which a load increase of 50 MPa was imposed for the subsequent load increment. The intent of increased load fatigue testing was primarily based on the suspicion that the LPBF microstructure contains failures by interlayer defects, unmolten particles and oxide inclusions as well as gas inclusions which may highly affect the lifetime endurance.

### 3.5 Microstructural analysis and hardness indentation

Prior to the examination, the samples were cut, embedded in epoxy resin, and finally polished with a diamond suspension of 1  $\mu\text{m}$ . After that, the sample microstructure was revealed

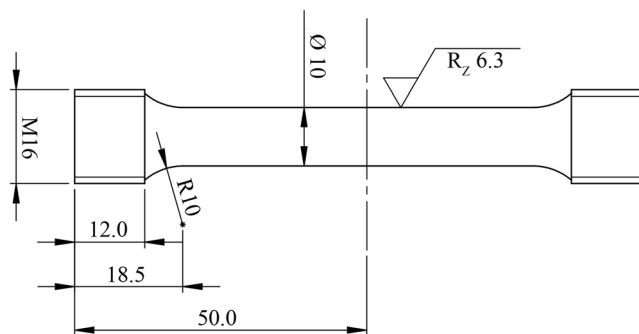


**Fig. 1** Geometry of the samples for strength characterization - type B10x50 according to DIN EN ISO 6892-1:2009-12

with a 2.5% Nital-etchant and analyzed using a digital light microscope type DMV6 (Leica Inc.) and a field emission scanning electron microscope type JSM 7001F (Jeol Inc.) with an integrated EDS detector (Oxford Inc.). In order to exclude the influence of a sputtered gold thin film for the EDS analysis of the brazed samples (AuNi18), conductive silver was always used instead in order to prevent electrical charging of the surface. Vickers hardness indentation was carried out on type 412A (Nexus Inc.) hardness tester with a test load of  $\text{HV}_{0.3}$ .

## 4 Results and discussions

### 4.1 Microstructure of the joints in the as-built condition

All LPBF joints can be described in accordance with the literature as regular, and as illustrated in Fig. 2, almost no failures were detected in the fusion area. The microstructure of the LPBF parts was substantially columnar and very fine cellular. A welding depth of around 50  $\mu\text{m}$  into the lower part was observed which was approximately the thickness of the applied layer height during building. The elongated areas in the light microscopic images of Fig. 2a–b result by the layer rotation of  $67^\circ$  and the randomly chosen cut level for the cross sections. For the LPBF/LPBF joints, the fusion area was just identifiable by the height of the existing and then remolten columnar microstructure as well as by a small overprint in diameter at the outline. In contrast to this, the fusion area of the LPBF/Conv. joints was easily detectable because the microstructure of the conventional part was not noticeably affected by the etchant. As shown in the SEM image in Fig. 2c, the etchant preferentially highlights the martensitic structures of the LPBF part which here appear whitish, so that according to Kučerová et al. an epitaxial growth of these martensitic structures was observed into the following solidification cell [1]. This was not visible at the interface to the conventional part which was of course expected because the unfused material was naturally still in the solution annealed condition.

### 4.2 Microstructure of the joints after heat treatment

In Fig. 3, the microstructure of the heat-treated LPBF/Conv. joints manufactured by LPBF as well as by vacuum brazing is shown.

After the solution annealing and precipitation hardening, it was not possible to detect the joint area of the LPBF/LPBF joints. In contrast to this, the additively manufactured part of the LPBF/Conv. joints was more affected by the etchant and much more inhomogeneous as the microstructure of the

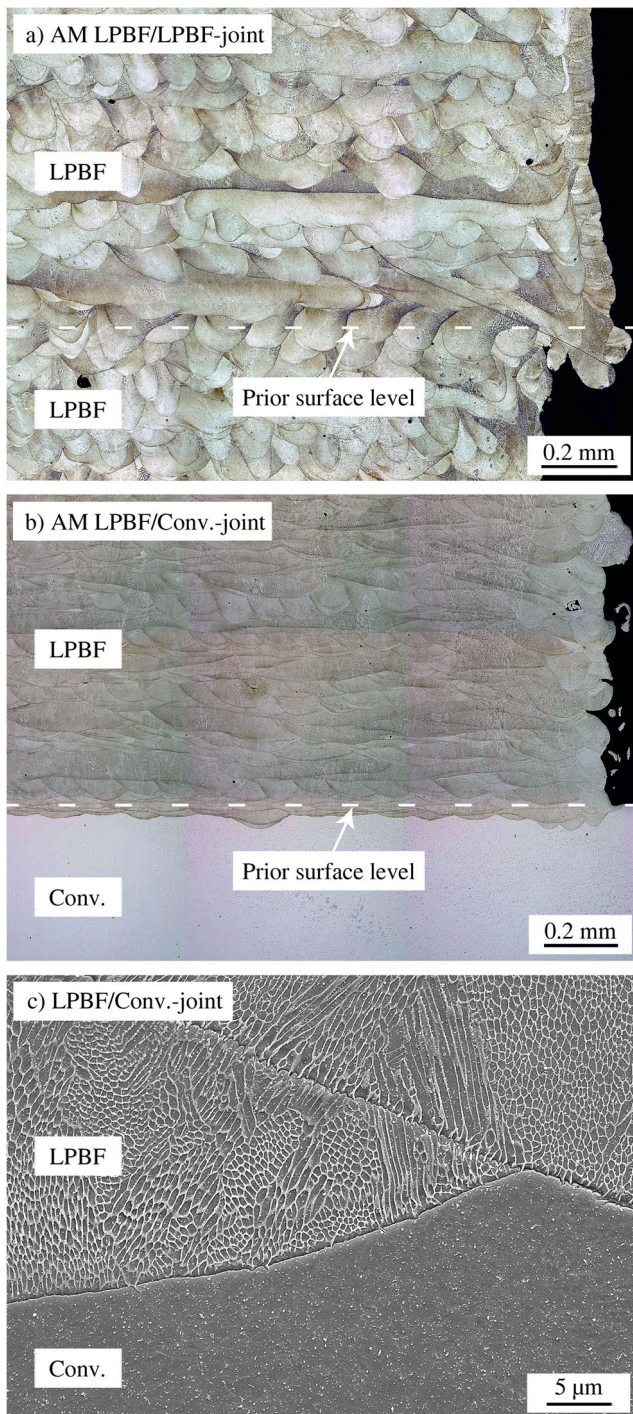


**Fig. 2** Microstructure of the additively manufactured joints (AM) in the as-built condition, etched with 2.5% Nital. **a, b** Light microscopic overview. **c** SEM image of the LPBF/Conv. joint area

conventional part (Fig. 3a). In the joint area, a smooth transition was observed between both martensitic microstructures. For the vacuum-brazed LPBF/Conv. joint, these microstructures were clearly separated by the braze metal for which not any failures were noticeable (Fig. 3b). In detail, the SEM/EDS analysis of such hybrid-brazed joints verifies the excellent suitability of the eutectic AuNi18 brazing filler metal for this

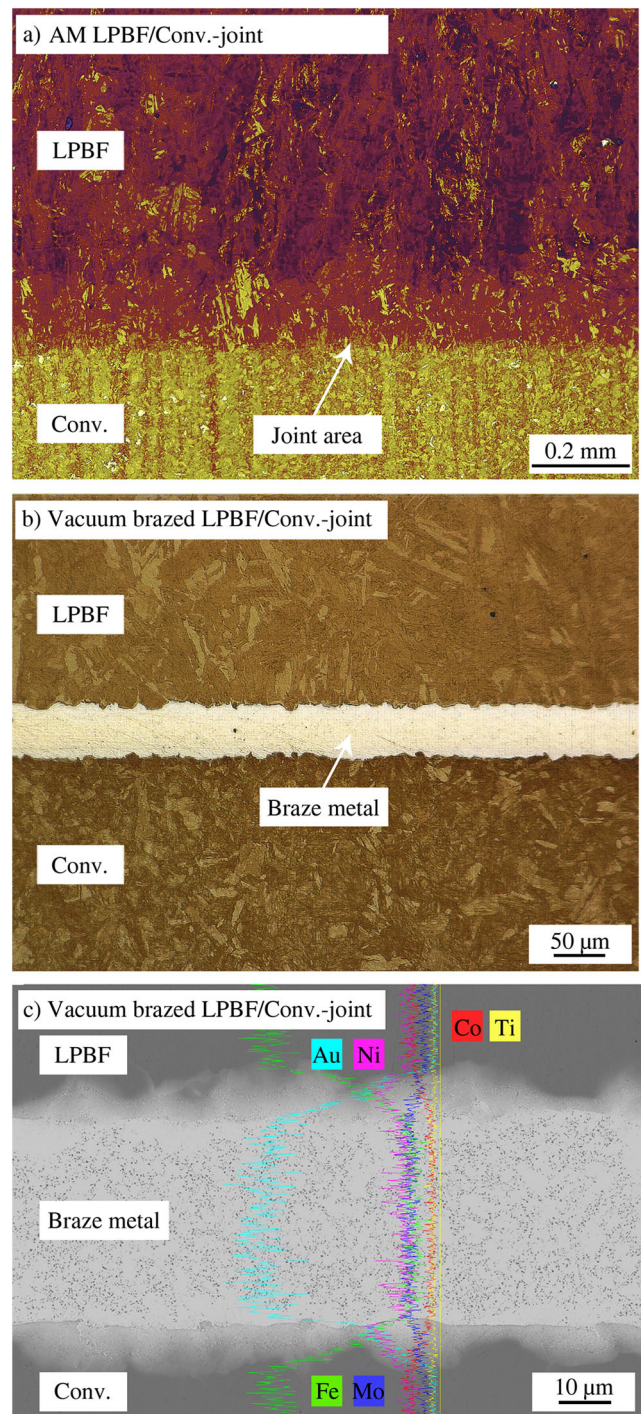


**Fig. 3** Microstructure of the additively manufactured (AM) and vacuum-brazed joints after heat treatment, etched with 2.5% Nital

joining task. As one can see in Fig. 3c, there was a similar microstructure and shaping of the diffusion area which is highly non-uniform at both interfaces of the braze metal to the base material. A very good metallurgical bond can be assumed by the qualitative EDS line scan and by the fact that the light gray-colored phase in the diffusion area was heavily enriched with nickel and gold, each up to 25 wt.-%. This was

expected since there is a high solubility in the ternary Fe-Ni-Au-phase diagram at 975 °C. The braze metal was a composition of the eutectic phase and a gold solid solution phase which was hardly identifiable by EDS due to its small size. However, this phase contained up to 7 wt.-% iron and up to 1.5 wt.-% molybdenum whereas almost no cobalt was detected. The fact that there was no significant difference for the LPBF/LPBF, LPBF/Conv., and Conv./Conv. joints supports this vacuum-brazing technology from the metallurgical view as a promising alternative manufacturing process for hybrid components of nickel maraging steels. Obviously, the additively manufactured joints showed an almost perfect joint quality.

### 4.3 Hardness of the joints

Extensive hardness measurements were carried out for the metallographic samples in the center line for which the indentation started close to the bottom and ended up close to the top of the sample. Therefore, an indent was set approximately every millimeter over the sample's height in order to investigate the effect of an increasing cooling time at longer buildup times on the hardness.

The result of this hardness trend over the sample height is illustrated in Fig. 4 for the additively manufactured LPBF/LPBF and LPBF/Conv. joints and for the as-built as well as for the solution annealed and precipitation-hardened condition. As one can see, the conventional part showed an almost constant hardness with an average of 328 HV<sub>0.3</sub>. It was clearly

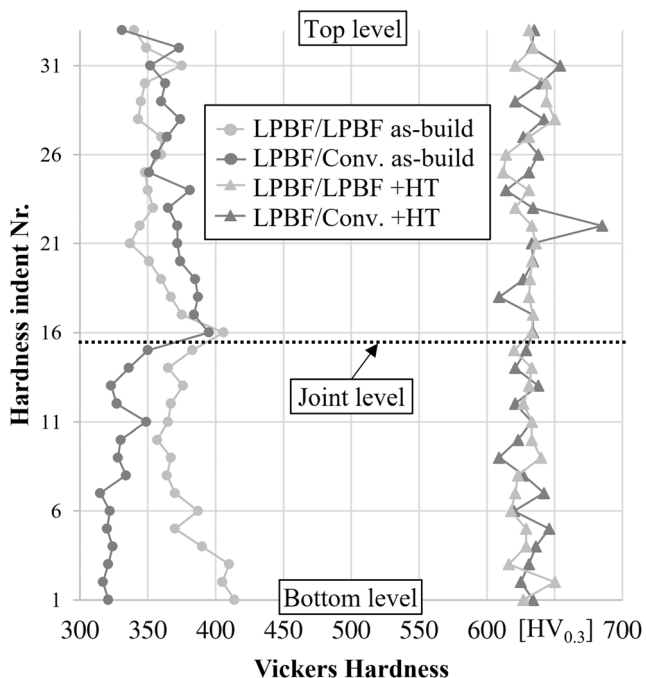


**Fig. 4** Vickers hardness measurement from the bottom of additively manufactured LPBF/LPBF and LPBF/Conv. samples in the as-built as well as in the heat-treated condition (HT)

visible that the hardness directly above the joint was the maximum hardness of 382 HV<sub>0.3</sub> and decreased approximately steadily with the buildup height to a minimum of 331 HV<sub>0.3</sub>. A similar behavior was investigated for the LPBF/LPBF joints for both parts. Hence, it was proven that the hardness of the LPBF part decreases with an increasing buildup height. The vacuum heat treatment process of solution annealing and precipitation hardening was approved to achieve a uniform hardness level, even for the hybrid LPBF/Conv. joint with an average hardness of 632 HV<sub>0.3</sub>.

### 4.4 Strength characterization

The results of tensile strength ( $R_m$ ) and increased load fatigue strength ( $R_{ILF}$ ) are summarized in Fig. 5. In the as-built condition, the single-processed LPBF samples achieved a tensile strength ( $R_m$ ) of 1073 MPa with a standard deviation ( $s$ ) of 68. In regard to this, the increased load fatigue strength was even slightly higher ( $R_{ILF}$ : 1150 MPa,  $s$ : 2). After the heat treatment, a significantly higher tensile strength was detected ( $R_m$ : 1618 MPa,  $s$ : 59) but there was a much lower increased load fatigue strength as well as an extraordinary high standard deviation ( $R_{ILF}$ : 1360 MPa,  $s$ : 488). In contrast to this, there was a proper tensile strength of 2154 MPa ( $s$ : 6) for the heat-

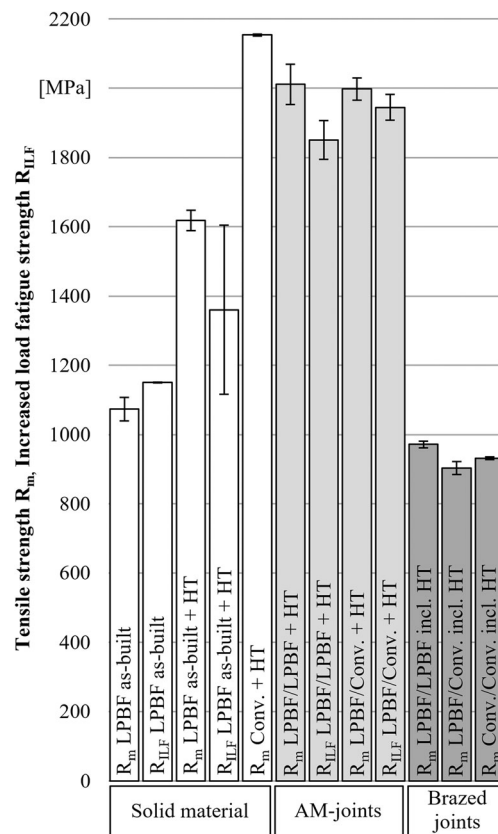


**Fig. 5** Tensile strength ( $R_m$ ) and increase load fatigue strength ( $R_{ILF}$ ) of solid material, additively manufactured joints (AM), or vacuum-brazed joints depending on the heat treatment condition (HT)

treated conventional material. Furthermore, there was a significant higher tensile strength for the additively manufactured LPBF/LPBF joints ( $R_m$ : 2011 MPa,  $s$ : 116) as well as for the LPBF/Conv. joints ( $R_m$ : 1998 MPa,  $s$ : 63) after heat treatment compared to the single processed LPBF samples. As expected, the increased load fatigue strength of these samples was just slightly lower ( $R_{ILF}$ : 1851 MPa,  $s$ : 113,  $R_{ILF}$ : 1945 MPa,  $s$ : 73). In a holistic view of these considerations, there were an unusually high number of macroscale failures within the LPBF microstructure which was clearly visible in the cross sections as interlayer defects and, thus, the strength was substantially affected. As a consequence of this, the given results must be evaluated with caution as the frequency of the interlayer defects differed quite a lot from sample to sample. However, it could be proven that the strength of additively manufactured joints was significantly higher compared to the single-processed LPBF samples in the heat-treated condition. Because of this, it is likely that the strength is decreased if there is a prolonged cooling time and that it is just not crucial if the sample cools down if the process interrupts overnight. Of course, in this case, the material should be preheated before continuing.

For the vacuum-brazed samples, there was no significant difference in tensile strength which was in average 972 MPa ( $s$ : 20) for the LPBF/LPBF joints, 904 MPa ( $s$ : 38) for the LPBF/Conv. joints, and 931 MPa ( $s$ : 8) for the Conv./Conv. joints which were used as a reference.

#### 4.5 Fracture analyses

As already expected by the explained results of the strength characterization, all additively manufactured samples fractured primarily due to a considerable volume of interlayer defects. This was clearly visible at the fractured surfaces by a locally shiny and golden-colored microstructure as well as by the cross sections as illustrated in Fig. 6a, b. In detail, there was a distinct constriction in diameter examined for the LPBF part of the samples so that it can be assumed that the plastic deformation in the mainly martensitic microstructure led to locally excessive stresses at the interlayer defects which act as a consequence of this as crack initiators. None of the samples fractured at the joint. In contrast to this, all the vacuum-brazed samples fractured completely within the braze metal (Fig. 6c). There was no significant difference in the fracture behavior between the LPBF/LPBF, LPBF/Conv., and Conv./Conv. joints which finally proves a very good suitability for vacuum brazing.

#### 5 Conclusion

The main conclusions are summarized below. It could be proven that vacuum brazing can be stated as a qualified

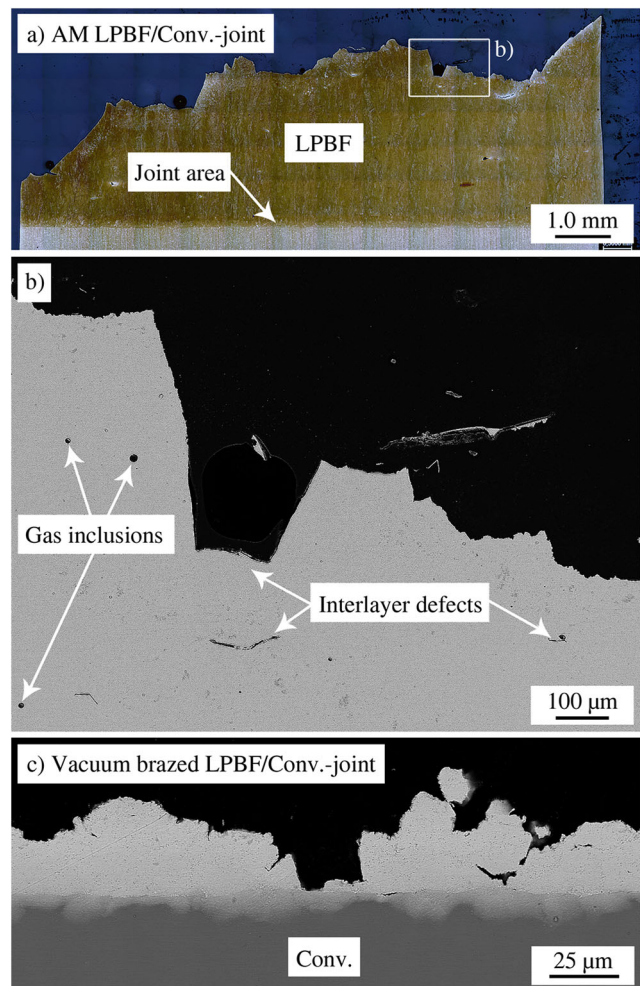


**Fig. 6** a, b Cross section fracture image of an additively manufactured (AM) and heat-treated LPBF/Conv. joint, etched with 2.5% Nital. c Cross section fracture image of a vacuum-brazed 18MAR300/AuNi18-joint

manufacturing method for hybrid joints of nickel maraging steel. The main advantage is given by the fact that the heat treatment of solution annealing and precipitation hardening can be easily united with the brazing in a single furnace run. This ended up in high strength joints with a tensile strength of more than 900 MPa which should be sufficient for many technical applications. In general, vacuum brazing is carried out as a batch process so that several joints can be manufactured simultaneously. However, in a holistic view, the substitution of high-volume component parts with conventional material can possibly enable more economical production costs compared to an exclusive manufacturing by laser powder bed fusion. Nevertheless, it was also shown that hybrid joints of nickel maraging steel 18MAR300 are also well processable by LPBF. The tensile strength of the joints can be given approximately by 2000 MPa in the heat-treated condition which is more than double than the vacuum-brazed ones. Furthermore, the results of increased load fatigue testing prove

that even several interlayer defects assure a very high strength of more than 1800 MPa. Finally, the given results facilitate engineers and designers to select the vacuum brazing or the LPBF process individually for an economical production of hybrid tools with respect to the particular stresses in the technical field of application.

**Code availability** Not applicable.

**Author contributions** T. Henning carried out the experiments as well as the analyses and wrote the manuscript with the support of W. Tillmann and L. Wojarski.

**Funding** Open Access funding enabled and organized by Projekt DEAL. German research foundation. Nr. “DFG TI 343/162-1,” title: “Brazeability of similar hybrid joint compounds consisting of additively manufactured and conventional material grades.”

**Data Availability** All data and samples are stored in accordance with the guidelines of the german research foundation and can be made available on request.

## Declarations

**Conflict of interest** The authors declare no competing interests.

**Open Access** This article is licensed under a Creative Commons Attribution 4.0 International License, which permits use, sharing, adaptation, distribution and reproduction in any medium or format, as long as you give appropriate credit to the original author(s) and the source, provide a link to the Creative Commons licence, and indicate if changes were made. The images or other third party material in this article are included in the article's Creative Commons licence, unless indicated otherwise in a credit line to the material. If material is not included in the article's Creative Commons licence and your intended use is not permitted by statutory regulation or exceeds the permitted use, you will need to obtain permission directly from the copyright holder. To view a copy of this licence, visit <http://creativecommons.org/licenses/by/4.0/>.

## References

- Kučerová L, Zetková I, Jandová A, Bystrianský M (2019) Microstructural characterization and in-situ straining of additive-manufactured X3NiCoMoTi 18-9-5 maraging steel. *Mater Sci Eng A* 750:70–80
- Bradshaw JF, Sandefur PG, Young CP Jr (1991) Braze alloy process and strength characterization studies for 18 nickel grade 200 maraging steel with application to wind tunnel models. National Aeronautics and Space Administration (NASA), Technical Memorandum 104075
- Afkhami S, Dabiri M, Habib Alavi S et al (2019) Fatigue characteristics of steels manufactured by selective laser melting. *Int J Fatigue* 122:72–83
- Thijs L, van Humbeeck J, Kempen K et al (2012) Investigation on the inclusions in maraging steel produced by selective laser melting. *Virtual Phys Prototyp*:297–304
- Kempen K, Yasa E, Thijs L, Kruth JP, van Humbeeck J (2011) Microstructure and mechanical properties of selective laser melted 18Ni-300 steel. *Phys Procedia* 12:255–263
- Schröder M, Falk B, Schmitt R (2015) Evaluation of cost structures of additive manufacturing processes using a new business model. *Procedia CIRP* 30:311–316
- Oyesola M, Mpofo K, Mathe N (2019) A techno-economic analytical approach of laser-based additive manufacturing processes for aerospace application. *Procedia Manuf* 35:155–163
- Tomas DS, Gilbert SW (2014) Costs and cost effectiveness of additive manufacturing. NIST Special Publication 1176. <https://doi.org/10.6028/NIST.SP.1176>
- Gutowski T, Jiang S, Cooper D et al (2017) Note on the rate and energy efficiency limits for additive manufacturing. *J Ind Ecol* 21: 69–79
- Rehm GM (2015) Chancen und Einschränkungen – Generative Fertigung für den Formenbau. *KunststoffXtra*, May:26–27
- Hoelker R, Tekkaya AE (2016) Advancements in the manufacturing of dies for hot aluminum extrusion with conformal cooling channels. *J Adv Manuf Technol* 83:1209–1220
- Malca C, Santos C, Sena M, Mateus A (2018) Development of SLM cellular structures for injection molds manufacturing. *Mater Sci Technol* 30:13–22
- Kučerová L, Zetková I, Jeniček Š, Burdová K (2020) Hybrid parts produced by deposition of 18Ni300 maraging steel via selective laser melting on forged and heat treated advanced high strength steel. *Addit Manuf* 32:101108
- Giganto S, Zapico P, Castro-Sastre MÁ, Martínez-Pellitero S, Leo P, Perulli P (2019) Influence of the scanning strategy parameters upon the quality of the SLM parts. *Procedia Manuf* 41:698–705
- Ferreira JAM, Santos LMS, da Silva J, Costa JM, Capela C (2016) Assessment of the fatigue life on functional hybrid laser sintering steel components. *Procedia Struct Integr* 1:126–133
- Metelkova J, Kinds Y, Kempen K, de Formanoir C, Witvrouw A, van Hooreweder B (2018) On the influence of laser defocusing in selective laser melting of 316L. *Addit Manuf* 23:161–169
- Bouzakis E, Arvanitidis A, Kezelis F et al (2020) Comparison of additively manufactured vs. conventional maraging steel in corrosion-fatigue performance after various surface treatments. *Procedia CIRP* 87:469–473
- Azizi H, Ghiaasiaan R, Prager R, Ghoncheh MH, Samk KA, Lausic A, Byleveld W, Phillion AB (2019) Metallurgical and mechanical assessment of hybrid additively-manufactured maraging tool steels via selective laser melting. *Addit Manuf* 27:389–397
- Lang FH, Kenyon N (1971) Welding of maraging steels. *WRC Bull* 159
- Tillmann W, Wojarski L, Henning T (2018) Vacuum brazing of 316L stainless steel based on additively manufactured and conventional material grades. *IOP Conf Ser: Mater Sci Eng* 373:012023. <https://doi.org/10.1088/1757-899X/373/1/012023>
- Shamantha CR, Narayanan R, Iyer KJL, Radhakrishnan VM, Seshadri SK, Sundararajan S, Sundaresan S (2000) Microstructural changes during welding and subsequent heat treatment of 18Ni (250-grade) maraging steel. *Mater Sci Eng A* 287:43–51
- Filho VXL, Barros I, de Abreu HFG (2017) Influence of solution annealing on microstructure and mechanical properties of maraging 300 steel. *Mater Res* 20(1):10–14



23. Casati R, Lemke JN, Tuissi A, Vedani M (2016) Aging behavior and mechanical performance of 18-Ni 300 steel processed by selective laser melting. *Metals* 6:218
24. Ullah R, Akmal JS, Laakso S, Niemi E (2020) Anisotropy of additively manufactured 18Ni-300 maraging steel: threads and surface characteristics. *Procedia CIRP* 93:68–78
25. Tillmann W, Henning T, Boretius M (2019) Effect of the dwell time on the microstructure and tensile strength of vacuum-brazed tool steels using B-Ni2 filler metal. *M Weld World* 63:1477–1488. <https://doi.org/10.1007/s40194-019-00734-z>
26. Reinkensmeyer I, Blank R, Hermann O (2019) Brazing of SLM-manufactured turbine components of the hot gas range from nickel alloys – differences in the diffusion behavior compared to conventional alloys. *Schweißen Schneiden* 71:214–220
27. Tillmann W, Wojarski L, Henning T et al (2019) The effect of nickel-plated surfaces on the microstructure and strength of vacuum brazed nickel maraging steel. In: 12<sup>th</sup> International Conference on Brazing, High Temperature Brazing and Diffusion Bonding, 21<sup>st</sup> to 23<sup>rd</sup> May, DVS-Berichte Band, vol 353. Aachen, Germany, pp 18–25
28. Reddy AN, Srinivasan D (2019) Small scale mechanical testing for additively manufactured (direct metal laser sintered) monolithic and hybrid test samples. *Procedia Struct Integr* 14:449–466
29. Hou H, Qi L, Zhao YH (2013) Effect of austenitizing temperature on the mechanical properties of high-strength maraging steel. *Mater Sci Eng A* 587:209–212
30. Berry RD (1965) Joining 18 per cent nickel maraging steel. *Weld Met Fabr* 3:93–95

**Publisher's note** Springer Nature remains neutral with regard to jurisdictional claims in published maps and institutional affiliations.